Uniformity and bandgap engineering in hydrogenated nanocrystalline silicon thin films by phosphorus doping for solar cell application

K. H. Li and W. Z. Shen[a)]
Department of Physics, Laboratory of Condensed Matter Spectroscopy and Opto-Electronic Physics, Institute of Solar Energy, Shanghai Jiao Tong University, 1954 Hua Shan Road, Shanghai 200030, China

(Received 23 May 2009; accepted 9 August 2009; published online 18 September 2009)

Micro-Raman mapping with a spatial resolution of micrometer and room-temperature visible photoluminescence (PL) has been carried out on phosphorus-doped hydrogenated nanocrystalline silicon (nc-Si:H) thin films grown by plasma enhanced chemical vapor deposition. Both the thin film uniformity and structural properties, i.e., the distribution of grain sizes and crystalline volume fraction, with different doping concentrations are revealed and physically interpreted based on the growth mechanism. The observed uniformity has been further confirmed by the PL measurements, and the bandgap engineering of the nc-Si:H thin films has been discussed from the dependence of PL peak energy on doping concentration. These results provide implications to realize control of properties of nc-Si:H by P-doping under optimized growth conditions for solar cell application. © *2009 American Institute of Physics*. [doi:10.1063/1.3223328]

I. INTRODUCTION

Due to their advantages over the first generation crystalline Si solar cells in ease of large area and low manufacturing cost, the second generation thin film solar cells, especially those based on Si, have attracted much attention and are ready to make a substantial contribution to the world's photovoltaic market.[1] For commercial amorphous Si (*a*-Si) thin films, however, there still remain some unavoidable disadvantages, i.e., low energy conversion efficiency,[2] low conductance, and light induced degradation of cell performance (the so-called Staebler–Wronski effect).[3] Nanocrystalline Si (nc-Si) thin film, a mixed-phase material consisting of nanocrystals embedded in amorphous tissue, presents very promising features in solving these problems.[1] Extensive optical and electrical investigations of nc-Si thin films have been carried out.[4–9] Strong optical absorption and high photocurrent are found in nc-Si films and attributed to the enhancement of the optical absorption cross section and good carrier conductivity in the nanometer grains.[10] There are numbers of attempts to realize high efficiency and good stability single-junction[11,12] and tandem[1,13,14] third generation nc-Si thin film solar cells.

Uniform deposition over a large area, which is one of the principle challenges in applying nc-Si thin film on an industrial scale, plays a significant role in promoting the performance of solar cells. Another critical factor that influences the performance of nc-Si solar cells is the controllable optical bandgap of nc-Si to make full use of the sunlight. In this paper, we investigate the effect of doping concentration in hydrogenated nc-Si (nc-Si:H) on both the thin film uniformity and optical bandgap with the aid of room-temperature Raman mapping and photoluminescence (PL) measurements. We emphasize the effect of phosphorus doping on the structural properties, including the grain size, crystalline volume fraction, and the distribution of grain sizes, together with the optical properties. The uniformity of the films versus doping concentration is discussed in terms of the growth mechanism.

II. SAMPLE PREPARATION AND EXPERIMENTS

The studied *n*-type nc-Si:H thin films were grown on undoped crystalline Si (111) substrates at a temperature of 250 °C by plasma enhanced chemical vapor deposition (PECVD). During the deposition, the radio frequency (13.56 MHz) power of 60 W and the total pressure of reactive gases of 0.7 Torr were maintained. Phosphine (PH_3) was used as dopant gas. The percentage content of phosphine (PH_3/SiH_4) C_P ranged from 0% to 20%, while the hydrogen dilution ratio $[H_2/(SiH_4+H_2)]$ was kept constant at 99%. The Si nanocrystal thin film has a layer thickness of around a few micrometers. The room-temperature electron mobility and dark conductivity of the nc-Si:H films reach in the order of 10^2 cm^2/Vs and 10 $S\ cm^{-1}$, respectively.[4]

Unpolarized micro-Raman mapping was performed on a Jobin Yvon LabRam HR800 UV micro-Raman spectrometer at room temperature. The measurements were carried out in backscattering configuration using an exciting wavelength of 514.5 nm from an Ar^+ laser. The laser light was focused onto the sample surface with a ×50 objective to produce a beam of diameter of 1 μm at the focal point. The Raman point-by-point mapping spectra of our nc-Si:H samples, mounted on a high precision motorized *X-Y* stage, were measured over randomly selected 10×10 μm^2 scan area with a step size of 1 μm along both the *x* and *y* directions and 100 Raman scattering spectra were taken for each sample. PL spectra of our samples were collected by the same spectrometer system at room temperature also with the sample points randomly selected.

[a)]Author to whom correspondence should be addressed. Electronic mail: wzshen@sjtu.edu.cn.

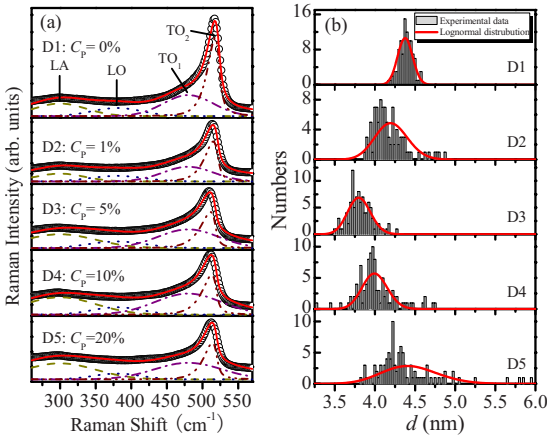

FIG. 1. (Color online) (a) Experimental (open circles) and fitted (solid curves) Raman spectra for samples D1–D5 with different phosphorus doping concentrations C_P. (b) Experimental histogram of the grain size d, together with the fitted lognormal distribution (solid curves).

III. RESULTS AND DISCUSSION

We start with Raman analyses to get information about the structures of our P-doped nc-Si:H thin films. We have randomly measured the Raman spectra of several spots for every sample before mapping, and the spectra of every sample are similar, which assures that the samples are uniform to some extent in large scale. By setting the mapping steps at 1 μm with the diameter of the laser beam being $\sim$1 μm, we have fully examined the properties of a randomly selected 10×10 μm^2 region with no overlapped area, which can sufficiently present the uniformity of the whole samples. In Fig. 1(a), we show the average spectra (open circles) of the total 100 experimental Raman spectra of each sample. The experimental Raman scattering spectra are decomposed into three Gaussian phonon bands [i.e., longitudinal acoustic (LA) band centered at 300 cm^{-1}, longitudinal optical (LO) band at 380 cm^{-1}, and transverse optical (TO$_1$) band at 480 cm^{-1}] from amorphous silicon contribution, and one asymmetric Lorentz shaped TO$_2$ band peaks at $\sim$520.5 cm^{-1} related to the nanocrystalline silicon. In terms of fitting the asymmetry TO$_2$ band peaks of crystalline Si, we employ the three-dimensional phonon confinement model,[15] which takes into account both the phonon confinement and the effect of strain. The intensity of the first order Raman spectrum is given by

$$I_{\mathrm{TO}_2}(\omega) = I_{0_{\mathrm{Raman}}} \int_0^{2\pi/a_0} \frac{|C(q)|^2 4\pi q^2 dq}{[\omega - \omega(q)]^2 + (\Gamma/2)^2}, \quad (1)$$

with $I_{0_{\mathrm{Raman}}}$ the prefactor, $|C(q)|^2=\exp(-q^2L_0^2/8)$ for spherical shape grain, L_0 the correlation length related to the average size of Si nanocrystallites, q the wave vector of phonon, Γ the Raman intrinsic linewidth of crystalline silicon, and a_0 =0.5483 nm the lattice constant of the bulk Si. The phonon dispersion relation $\omega(q)$ is taken according to Ref. 16:

$$\omega(q) = \omega_p - 120(q/q_0)^2, \quad (2)$$

where ω_p is the wavenumber of the first order Raman band in the absence of disorder effects and $q_0=2\pi/a_0$.

Good agreement has been achieved between the calculated (solid curves) and experimental Raman spectra. The Si grain size d can be estimated from the fitting parameter L_0, which corresponds to the average distance between defects, by $d=L_0/a_0$ in the case of low amount of defects.[17,18] Simultaneously, the crystalline volume fraction X_C can be also obtained by using $X_C=I_{\mathrm{TO}_2}/(I_{\mathrm{TO}_2}+\gamma I_{\mathrm{TO}_1})$, where $\gamma(L_0)=0.1+\exp(-L_0/25)$ with I_{TO_1} and I_{TO_2} the integrated intensities of TO$_1$ and TO$_2$ bands, respectively.[19,20] Both the average grain size d and the average crystalline volume fraction X_C determined from the 100 Raman spectra are presented in Table I. We notice the first gradual decrease in the average grain size d when C_P increases up to 5%, and then the gradual increase with the further increase in C_P, whereas the average crystalline volume fraction X_C decreases continuously from 54.9% to 35.4% as C_P increases from 0% to 20%.

In order to reveal unambiguously the nonuniformity of the nc-Si:H thin films, we have illustrated in Fig. 1(b) the distribution of grain size from the Raman mapping spectra, together with a lognormal distribution function fitting at the peak position of the average grain size d. Both the normal and lognormal distribution fittings have been performed and the latter one shows a better agreement with the experimental data. From Fig. 1(b), we can identify easily the change in the average grain size and the linewidth of the distribution, which indicates the standard deviation, with the doping concentration. Table I lists the corresponding relative deviation $\sigma_{\mathrm{Raman}}/d$, through dividing the standard deviation of the distribution σ_{Raman} by the average grain size d, to reveal the nonuniformity of the nc-Si:H thin films. It is clear that there are small relative deviations in all these nc-Si:H thin films, demonstrating the good uniformity of the samples. The intrinsic sample D1 exhibits the narrowest linewidth in the

TABLE I. Parameters for the series of lightly P-doped nc-Si:H thin films. C_P is the phosphorus doping concentration (PH_3/SiH_4). d, X_C, and $\sigma_{\mathrm{Raman}}/d$ are the average grain size, crystalline volume fraction, and relative deviation obtained from Raman spectra. $I_{0_{\mathrm{PL}}}$, σ_{PL}/d, C, I_{peak}, and E_{gPL} are the proportional constant, relative deviation, QC-related parameter, peak intensity, and peak position calculated from PL spectra, respectively.

Samples	C_P (%)	d (nm)	X_C (%)	$\sigma_{\mathrm{Raman}}/d$ (%)	$I_{0_{\mathrm{PL}}}$	σ_{PL}/d (%)	C	I_{peak}	E_{gPL} (eV)
D1	0	4.4	54.9	1.88	38.29	2.78	19.46	3237.8	1.918
D2	1	4.2	43.4	4.70	28.04	3.58	19.74	1688.2	1.948
D3	5	3.8	37.7	3.56	62.66	3.51	15.66	3490.1	1.963
D4	10	4.0	35.8	3.74	39.29	3.61	17.27	2278.0	1.933
D5	20	4.4	35.4	7.77	14.78	4.21	21.63	870.5	1.859

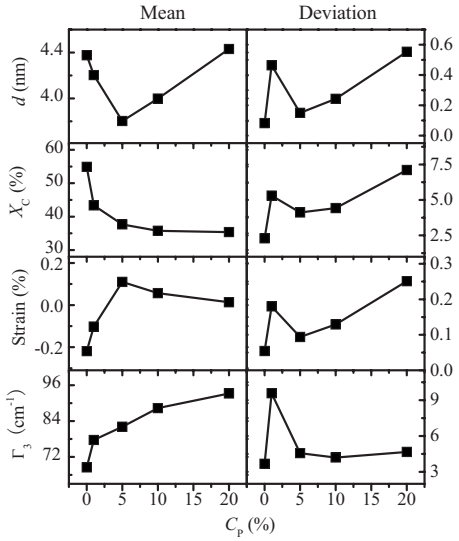

FIG. 2. Mean values and standard deviations of the average grain size d, crystalline volume fraction X_C, intrinsic compressive strain, and linewidth Γ_3 of the amorphous TO_1 band at 480 cm^{-1} with respect to the phosphorus doping concentrations C_P.

distribution profile, i.e., the most homogeneous with the least relative deviation of only 1.88%, while in doped samples, the relative deviation (thin film nonuniformity) first decreases and then enhances with increasing doping concentration. Theoretical and experimental reports all conclude that the size distribution parameters d and σ_{Raman} of Si:H thin films resulting from differences in deposition conditions play an important role in the device performance[5,21] and, in particular, the stability of the corresponding solar cells.

We present in Fig. 2 the dependence of both statistical mean values and standard deviations on doping concentration C_P for the grain size d, the crystalline volume fraction X_C, as well as the linewidth Γ_3 of the amorphous TO_1 band and the strain. Γ_3 is yielded directly by the Raman lineshape fitting procedure, while the strain is simply calculated by $-(\omega_p-\omega_0)/3\xi\omega_0$, with ω_0 the wavenumber of the first order Raman band in the absence of both disorder and stress effects (520.5 cm^{-1}) and ξ the Grüneisen constant ($\sim$1.0).[15] Interestingly, the mean values of d and X_C appear to have an opposite dependence on C_P to those of strain and Γ_3, respectively. It is not difficult to understand this result from their close relation point of view. The lattice distortion occurred at the interface of the nanocrystallites causes the strain. Small grain corresponds to large surface volume ratio, leading to the opposite tendency of d and strain with respect to C_P. On the other hand, Γ_3, being linearly proportional to bond-angle variation in an a-Si:H network, can serve as a useful qualitative indicator of the degree of short-range disorder,[22] whereas X_C is indicative of the degree of short-range order. The observed behavior of X_C and Γ_3 in Fig. 2 demonstrates that increasing doping concentration reduces the degree of structural order within these nc-Si:H thin films.

The yielded statistical standard deviation is closely related to the uniformity of the samples. It is clear that the standard deviation of all the four quantities for d, X_C, strain, and Γ_3 in Fig. 2 exhibit the similar dependence on the doping concentration C_P. The intrinsic sample has the least standard deviation, therefore is the most uniformed one, while by increasing or decreasing the doping concentration from C_P =5%, there is a gradual increase in the standard deviation of the doped nc-Si:H films. We discuss the observation from the framework of growth mechanism and the role of the grain size fluctuation. The introduction of dopant phosphor causes the lattice distortion and results in the disorder in the films. However, the standard deviation does not increase monotonically with the enhancement of C_P, which can be interpreted in terms of the difference between the concept of structural order and uniformity. Uniformity represents macroscopical properties of the material, while structural order correlates to microcosmic properties. One typical example is that disordered amorphous silicon can be more homogeneous than highly ordered crystal silicon.

In the low doping concentration (C_P below 5%), the increase in disorder hinders the crystallization of nanocrystalline silicon, as revealed by the smaller grain size d and lower crystalline volume fraction X_C under the higher doping concentration. The lower X_C suggests more amorphous phase in higher doped samples, which leads to the enhancement of macroscopical uniformity. However, with the further doping of phosphor for C_P over 5%, the lattice distortion becomes much more sever; hence, the fluctuation of the nanocrystallites density is more obvious in spatial. That is to say, some area holds more nanocrystallites than others, leading to the aggregation of several neighboring grains in "condensed" area, and gives rise to the increasing grain size d with slow decrease in the crystalline volume fraction X_C. The thin film uniformity is therefore reduced with the increase in doping concentration. For the stable performance of solar cells, the industry always requires the large scale uniformity of the material. The results presented above show the remarkable impacts of doping on the uniformity, which reminds us that in pursuing the good electric and optical properties of nc-Si:H thin film solar cells by doping, we should also take into account carefully its effect on the thin film uniformity.

In order to gain more insight into the optical properties such as the bandgap of these nc-Si:H thin films, we present in Fig. 3(a) the experimental (open circles) room-temperature PL spectra of the five P-doped nc-Si:H with different C_P. All the PL spectra, which are normalized at their maximum intensities and shifted vertically for clarity, shows broad luminescence band in the visible light region from 1.859 to 1.963 eV. The PL profiles can be well reconstructed by using the model (solid curves) proposed by Islam and Kumar (IK model),[23] which takes into account the combined effects of quantum confinement (QC),[24–26] localized surface states,[27,28] and grain size distribution, together with a lognormal rather than normal crystallite size distribution. It should be noted that we have performed both the normal and lognormal distribution fittings and chose the latter one by considering its better agreement with the experimental data. This argument is also in good agreement with the Raman analyses in Fig. 1(b).

As deduced by the IK model, the expression for PL intensity for a lognormal distribution is

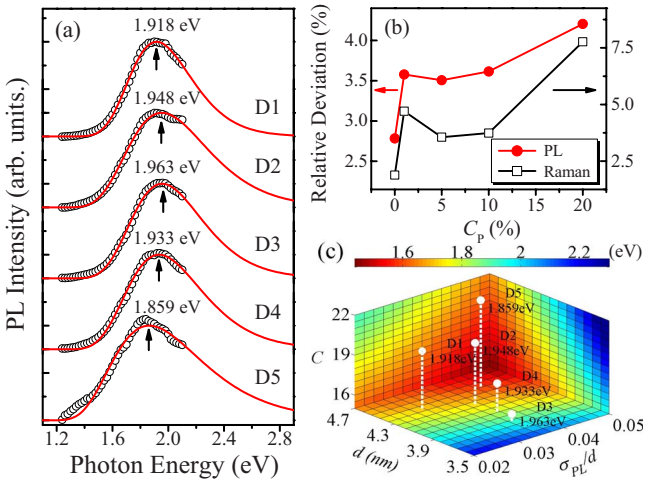

FIG. 3. (Color online) (a) Experimental (open circles) and calculated (solid curves) PL spectra for samples D1–D5. The PL spectra have been shifted vertically for clarity. (b) Relative deviation σ_{PL}/d and σ_{Raman}/d vs C_P calculated from PL and Raman spectra, respectively. (c) Luminescence peak energy E_{gPL} as a function of d, σ_{PL}/d, and C by computer simulations, together with the experimental data (circles).

$$I(\Delta E) = I_{0_{PL}} \frac{(C/\Delta E)^{(5-\alpha+n)/n}}{nC\sigma_0} \times \exp\left[-\frac{\{\ln(C/\Delta E)^{1/n} - \ln(d_0)\}^2}{2\sigma_0^2}\right], \quad (3)$$

with $I_{0_{PL}}$ the proportional constant, d_0 the median grain size of the distribution, σ_0 describing the size dispersion, and $\Delta E = C/d_0^n$ the amount of bandgap widening due to the QC effect. In the case of lognormal distribution, the average grain size is given by $d = d_0 \exp(\sigma_0^2/2)$ and standard deviation of the distribution σ_{PL} equals to $d\{\exp(\sigma_0^2)/2\}$. During the PL profile fitting, we only vary $I_{0_{PL}}$, σ_0, and C, and use the Raman-yielded average grain size d values. The value of α is taken from the literature,[23] with $n=2$ estimated from the effective mass theory.[29] Table I lists the fitting results $I_{0_{PL}}$, σ_{PL}/d, and QC-related parameter C, together with the peak intensity I_{peak} and peak position E_{gPL}.

We have correlated in Fig. 3(b) the change in the relative deviation σ_{PL}/d from PL spectra (filled circles) with the Raman ones (open squares). Obviously, the relative deviation deduced from the PL spectra coincides fairly well with those from Raman measurements, clearly demonstrating the reliability of those two methods. Extra attention should be paid to the fact that σ_{Raman}/d is larger than σ_{PL}/d in general, which can be well elucidated in terms of the basic difference between these two quantities. σ_{Raman}/d, acquired from 100 Raman spectra taken at different spots, definitely contains the information of both the uniformity of the films and the distribution of grain size, whereas σ_{PL}/d is taken at one PL spectrum of a randomly selected spot and only includes the deviation caused by grain size distribution. From this point of view, it is reasonable to predict that there is little value difference between σ_{PL}/d and σ_{Raman}/d for highly homogeneous films with low standard deviation, as is confirmed by our observation. The highly consistency between the PL and Raman analyses validates that the IK model is a satisfactory method to reveal the size dispersion in nanomaterials. Moreover, the Raman mapping can effectively distinct information on the thin film uniformity, which is indispensable in solar cell evaluation from the viewpoints of both fundamental physics and future applications.

The PL spectra in Fig. 3(a) also reveal the dependence of doping concentration on the luminescence peak position E_{gPL} in nc-Si:H films: The peak position blueshifts with increasing C_P until reaching a maximum at about 1.963 eV, and then it redshifts at higher C_P. From the IK model, the shift of the luminescence peak with doping concentration depends sensitively on the localized surface states, the grain size distribution, and the QC effect, which gives rise to PL in the visible region for crystallite sizes below ~5 nm. There are mainly three parameters, i.e., d, σ_{PL}/d, and C, which affect the PL peak energy. Since the PL peak energy is closely related to the optical bandgap,[21,30] which is one of the most important optical properties of nc-Si:H thin film solar cells, we exhibit in Fig. 3(c) the variation in E_{gPL} with d, σ_{PL}/d, and C by computer simulations, where the experimental PL data have been exhibited as well (circles). In Fig. 3(c), different peak positions are denoted by different colors, with red that corresponds to lower peak energy and blue to higher one. It is quite explicit that E_{gPL} redshifts with an increase in d and σ_{PL}/d, while it blueshifts with an enhancement of C. Thus it is important to consider the coaction of these factors in tuning the optical band gap by controlling the deposition parameters to make an ideal match with the terrestrial solar spectrum for maximum efficiency of the nc-Si:H thin film solar cells.

IV. CONCLUSIONS

In summary, the structural and optical properties of nc-Si:H thin films grown by PECVD have been investigated by micro-Raman mapping and PL measurements. By the aid of the statistical method for the grain size and crystalline volume fraction obtained by the three-dimensional phonon confinement model of the Raman spectra, we are able to reveal both the average quality and the material uniformity of the nc-Si:H thin films in relation to the doping concentration. The PL profiles, well reproduced by the IK model, yield microstructural information in good agreement with the Raman analysis, demonstrating that PL spectrum is a convenient method to acquire the size dispersion, while the Raman mapping can further identify the thin film uniformity in nanomaterials. Additionally, we have investigated the shift of the PL peak energy stemming from the variation in P-doping concentration, which is determined by the values of d, σ_{PL}/d, and C. Therefore, selection of appropriate doping concentration allows the production of samples exhibiting high uniformity and suitable optical bandgap. We expect that this study may benefit to the improvement of the nc-Si:H thin film solar cell performance, although controlling the growth conditions such as gas pressure, hydrogen dilution ratio, and substrate temperature, which are not independent of each other for optimizing the growth of nc-Si:H, still needs further investigations.

ACKNOWLEDGMENTS

This work was supported by the Natural Science Foundation of China (Contract No. 10734020), the National Major Basic Research (Project Nos. 2010CB933702 and 2006CB921507), and the Shanghai Municipal Commission of Science and Technology (Project No. 08XD14022).

[1]J. Yang, B. J. Yan, and S. Guha, Thin Solid Films **487**, 162 (2005).
[2]Photovoltaic Technology Research Advisory Council (PV-TRAC), A Vision for Photovoltaic Technology for 2030 and Beyond, Photovoltaic Technology Research Advisory Council (PV-TRAC), European Communities, 2004.
[3]D. L. Staebler and C. R. Wronski, Appl. Phys. Lett. **31**, 292 (1977).
[4]X. Y. Chen, W. Z. Shen, and Y. L. He, J. Appl. Phys. **97**, 024305 (2005).
[5]H. Chen and W. Z. Shen, Appl. Phys. Lett. **88**, 121921 (2006).
[6]X. Y. Chen and W. Z. Shen, Phys. Rev. B **72**, 035309 (2005).
[7]W. Pan, J. J. Lu, J. Chen, and W. Z. Shen, Phys. Rev. B **74**, 125308 (2006).
[8]J. J. Lu, J. Chen, Y. L. He, and W. Z. Shen, J. Appl. Phys. **102**, 063701 (2007).
[9]K. Zhang and W. Z. Shen, Appl. Phys. Lett. **92**, 083101 (2008).
[10]R. Zhang, X. Y. Chen, K. Zhang, and W. Z. Shen, J. Appl. Phys. **100**, 104310 (2006).
[11]A. Matsuda, J. Non-Cryst. Solids **338–340**, 1 (2004).
[12]Y. Mai, S. Klein, and F. Finger, Appl. Phys. Lett. **85**, 2839 (2004).
[13]B. Yan, G. Yue, J. M. Owens, J. Yang, and S. Guha, Fourth World Conference on Photovoltaic Energy Conversion, Waikoloa, HI, May 2006 (unpublished).
[14]K. Yamamoto, M. Yoshimi, T. Sawada, S. Fukuda, T. Suezaki, M. Ichikawa, Y. Koi, M. Goto, T. Meguro, T. Matsuda, M. Kondo, T. Sasaki, and Y. Tawada, Prog. Photovoltaics **13**, 489 (2005).
[15]M. Yang, D. M. Huang, P. H. Hao, F. L. Zhang, X. Y. Hou, and X. Wang, J. Appl. Phys. **75**, 651 (1994).
[16]Z. Sui, P. P. Leong, I. P. Herman, G. S. Higashi, and H. Temkin, Appl. Phys. Lett. **60**, 2086 (1992).
[17]H. Richter, Z. P. Wang, and L. Ley, Solid State Commun. **39**, 625 (1981).
[18]H. Campbell and P. M. Fauchet, Solid State Commun. **58**, 739 (1986).
[19]E. Bustarret, M. A. Hachicha, and M. Brunel, Appl. Phys. Lett. **52**, 1675 (1988).
[20]B. Garrido, A. Pérez-Rodr ĭ guez, J. R. Morante, A. Achiq, F. Gourbilleau, R. Madelon, and R. Rizk, J. Vac. Sci. Technol. B **16**, 1851 (1998).
[21]M. N. Islam and S. Kumar, Appl. Phys. Lett. **78**, 715 (2001).
[22]D. X. Han, J. D. Lorentzen, J. Weinberg-Wolf, L. E. McNeil, and Q. Wang, J. Appl. Phys. **94**, 2930 (2003).
[23]M. N. Islam and S. Kumar, J. Appl. Phys. **93**, 1753 (2003).
[24]L. T. Canham, Appl. Phys. Lett. **57**, 1046 (1990).
[25]V. Lehmann and G. Gosele, Appl. Phys. Lett. **58**, 856 (1991).
[26]L. P. Proot, C. Delerue, and G. Allan, Appl. Phys. Lett. **61**, 1948 (1992).
[27]V. Petrova-Koch, T. Muschik, A. Kux, B. K. Meyer, F. Koch, and V. Lehmann, Appl. Phys. Lett. **61**, 943 (1992).
[28]Y. Kanemitsu, Phys. Rev. B **49**, 16845 (1994).
[29]T. Y. Kim, N. M. Park, K. H. Kim, G. Y. Sung, Y. W. Ok, T. Y. Seong, and C. J. Choi, Appl. Phys. Lett. **85**, 5355 (2004).
[30]A. M. Ali, J. Lumin. **126**, 614 (2007).